Showcasing the first publication from Dr. Palas Roy's research laboratory, Department of Chemistry, Indian Institute of Technology Bhubaneswar, Odisha, India.

Hydrogen-bonding environment suppresses thermally activated delayed fluorescence

Thermally activated delayed fluorescence (TADF) emitters power modern OLED displays, yet their brightness is extremely sensitive to their microscopic surroundings. We show that protic hydrogens directly interact with the photoexcited TADF emitter, distorting it out of its light-producing geometry and silently draining its emission. Strikingly, this quenching effect is universal across a range of TADF molecules, underscoring the generality of the phenomenon. Our findings reveal that precise control of local hydrogen-bonding environments is essential for achieving brighter, ultra-efficient next-generation OLED technologies.

Image reproduced by permission of Sushree Suhani Puhan from *Chem. Sci.,* 2026, **17**, 187.

Image created with Google Gemini.

As featured in:

See Palas Roy *et al.*, *Chem. Sci.,* 2026, **17**, 187.

ROYAL SOCIETY OF CHEMISTRY

rsc.li/chemical-science

Registered charity number: 207890

Chemical Science

ROYAL SOCIETY OF CHEMISTRY

EDGE ARTICLE

View Article Online
View Journal | View Issue

Cite this: *Chem. Sci.*, 2026, **17**, 187

All publication charges for this article have been paid for by the Royal Society of Chemistry

Hydrogen-bonding environment suppresses thermally activated delayed fluorescence

Sushree Suhani Puhan,[a] Laxmipriya Dash[bc] and Palas Roy *[a]

Thermally activated delayed fluorescence (TADF) is a promising innovation in display technology where the nonemissive triplet excitons can be thermally converted back into emissive singlet excitons through reverse intersystem crossing. Organic TADF emitters often feature donor–acceptor (D–A) architectures, whose conformations critically influence emission dynamics and efficiency. Introducing intramolecular hydrogen-bonding between D and A moieties is an emerging strategy to rigidify the structure and improve TADF emission. However the influence of environmental factors on such hydrogen-bonding interactions remains unclear. Here we investigate the impact of the hydrogen-bonding medium on TADF emission using steady-state and time-resolved emission spectroscopy. Protic solvents universally quench TADF emission, correlating with reduced prompt emission lifetimes, while delayed lifetimes remain largely unchanged. A clear kinetic isotope effect unequivocally confirms that solvent protons directly participate in hydrogen-bonding interactions with the photoexcited emitter, thereby perturbing its excited-state energetics. Ultrafast spectroscopy reveals a picosecond D-to-A intramolecular charge transfer event that slows in viscous media indicating a D–A torsional relaxation. The relaxation time further slows in a protic environment highlighting the role of solvent-emitter hydrogen-bonding interactions resulting in unfavourable excited state D–A conformations and diminished emission. These findings underscore the importance of microenvironment control in designing efficient TADF emitters for display applications and photocatalysis.

Received 24th July 2025
Accepted 24th November 2025

DOI: 10.1039/d5sc05548b

rsc.li/chemical-science

Introduction

Developing new materials for display and lighting technologies is a key challenge for the 21st century. The light emission process in an electroluminescent device involves injecting opposite charges which combine to form singlet and triplet excitons in a 1 : 3 ratio.[1] In most materials, triplets do not emit light, but for high efficiency, the triplets need to be harvested to contribute to light emission. The state-of-the-art organic light-emitting diode (OLED) technology achieves high efficiency by a process called thermally activated delayed fluorescence (TADF), which offers a tantalizing solution of efficiently converting these non-emissive triplets into emissive singlets thermally owing to nearly equivalent singlet and triplet energy levels.[2–4] Upon photoexcitation, TADF molecules initially generate a Franck–Condon singlet exciton (see Fig. 1), which undergoes relaxation and subsequently emits light on the nanosecond timescale (prompt emission).[1,5] In parallel, a portion of these singlet excitons undergoes intersystem crossing (ISC) to form triplet excitons which can be thermally activated and converted back into the radiative singlet manifold *via* reverse intersystem crossing (rISC), leading to emission on the microsecond timescale (delayed emission). Typically a suitable host matrix is used for housing the guest TADF emitters to help efficient transport of charge carriers, support exciton formation and prevent exciton quenching.[6–8] Such host

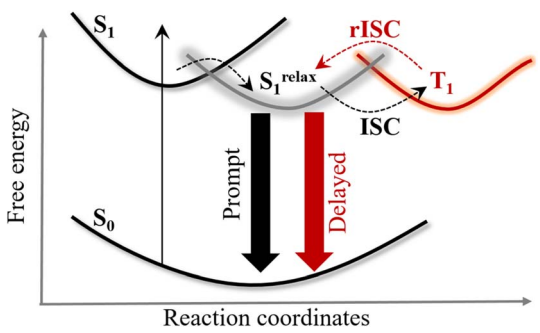

Fig. 1 Photophysical model of thermally activated delayed fluorescence (TADF) where absorption of light leads to the Franck Condon S_1 state which undergoes relaxation followed by emission of prompt photons. S_1 also undergoes intersystem crossing (ISC) leading to the nonemissive T_1 state which can be converted back into the S_1 state *via* reverse intersystem crossing (rISC) followed by emission of delayed photons.

[a]*Department of Chemistry, IIT Bhubaneswar, Argul 752050, India. E-mail: palasroy@iitbbs.ac.in*
[b]*School of Chemical Sciences, NISER Bhubaneswar, Khurda 752050, India*
[c]*Training School Complex, Homi Bhabha National Institute, Mumbai 400094, India*

materials consist of carbazole, triazine or phosphine oxide moieties for balanced charge flow.[9] Reorientation of the local environment in polymeric and small-molecule hosts was found to stabilize the TADF exciton.[10] Therefore factors such as polarity and viscosity of the surrounding environment significantly impact the ISC and rISC timescales and hence affect the emission properties of TADF materials.[11–15] However the challenge is finding the right host environment to ensure they complement the TADF emission and optimize performance of the OLEDs. In fact TADF materials are also emerging as novel photocatalysts where optimizing the right environment could play a crucial role in influencing the efficiency, selectivity, and stability of the reaction intermediates.[16,17]

Organic TADF molecules consist of donor (D) and acceptor (A) moieties where placement and conformation of these moieties are important for engineering their performance.[12,18–23] Tuning the D–A dihedral angle was found to affect the spin orbit coupling, ISC and rISC timescales.[24–26] Recently intramolecular hydrogen bonding in TADF materials has gained enormous interest as a means to tailor their emission behavior in solid films and crystalline environments.[27–31] By introducing hydrogen bonding interactions between donor and acceptor segments within a TADF chromophore, the rigidity of the molecular structure can be increased, which potentially hinders the D–A conformational changes and helps to reduce non-radiative decay and improves the overall emission quantum yield. Moreover, many host materials inherently contain electronegative atoms capable of forming H-bonding interactions in the solid state.[32–34] Therefore, host–emitter hydrogen-bonding interactions are not only possible, but can subtly modulate the molecular conformation, excited-state dynamics, and emission efficiency. However such interactions have been rarely studied and require a detailed investigation to further optimise TADF emission in next-generation OLEDs. Motivated by these insights, the present study systematically investigates and quantifies the role of the H-bonding environment in governing TADF emission and dynamics by comparing protic and aprotic solvent systems. We show that protic solvents induce pronounced quenching of TADF emission, distinct from general polarity or viscosity effects. This molecular-level understanding bridges the gap between environmental interactions and device-level performance and provides design principles for developing novel dopant and host molecules to boost the performance of advanced OLED devices.

Results and analysis

Steady-state electronic spectra

Here we choose a 2,4,5,6-tetrakis(9*H*-carbazol-9-yl) isophthalonitrile (4CzIPN) molecule (Fig. 2a) which is a well-known TADF emitter containing two cyano groups (acceptors) and four carbazole units (donors). The absorption and emission spectra of 4CzIPN in polar aprotic acetonitrile (ACN) are shown in Fig. 2b. The absorption spectra in ACN show maxima at 365 nm corresponding to the intramolecular charge transfer transition.[35] The emission spectra in ACN show maxima at 542 nm with a quantum yield (QY) of 0.20. In order to investigate the role of the H-bonding environment, we choose methanol (MeOH) that has similar polarity to ACN (see Table 1). The absorption maxima of 4CzIPN in MeOH are redshifted to 368 nm with broadened spectral width. Despite this spectral shift, the absorption spectra in both the solvents have similar shapes. The emission maxima in MeOH are red shifted to 549 nm with a QY of 0.12. Isopolarity of solvent ensures that such a huge drop in QY (by *ca.* 40%) is purely due to the H-bonding environment, but not due to solvent polarity. To reaffirm such behaviour, we recorded the absorption and emission spectra in the isopolar solvents aprotic acetone (ACE) and protic isopropanol (iPrOH). The absorption maxima of 363 nm in ACE are red shifted to 374 nm in iPrOH with broadened spectral width in iPrOH. On the other hand, the emission maxima and QY values are 532 nm and 0.4 respectively in aprotic ACE while these values are 543 nm and 0.24 respectively in protic iPrOH. Therefore protic solvent is playing a crucial role in the quenching of TADF emission.

To decouple the effects of polarity and viscosity from those of the protic environment, we conducted additional steady-state measurements in a series of isoviscous and isopolar solvents (see Table 1 for solvent parameters). Comparing absorption and emission spectra in isoviscous aprotic solvents (with increasing polarity) methyl acetate, acetone and ACN shows that the emission maxima, Stokes shift and the QY decreases with an increase in solvent polarity whereas the absorption maxima remain nearly unchanged (see, SI Fig. S1, S2a, Tables S2 and S3). Such Stokes shifted emission spectra indicate the polar character of 4CzIPN in the excited state. Plotting the solvent polarity factor *versus* emission Stokes shift shows that the excited state is highly polar in nature with a dipole moment of 20D (obtained from the Lippert Mataga plot in isoviscous solvent, see SI Fig. S3). To investigate the effect of viscosity, we recorded absorption and emission spectra in isopolar dimethyl acetamide (DMA) and *N*,*N*-dimethyl formamide (DMF) (as shown in SI Fig. S1, S2b, Tables S2 and S3), and compared that with ACN data. This suggests that the increase in solvent viscosity leads to slightly blue shifted emission spectra whereas the absorption maxima are nearly unchanged. The emission quantum yield of 0.2, 0.32 and 0.4 in ACN, DMF and DMA respectively suggests that the emission quantum yield increases with an increase in solvent viscosity. This behaviour is different to that obtained with protic solvents which significantly quenches the emission quantum yield. The absorption maxima being independent of solvent polarity and viscosity suggests that the relative changes in both ground and excited state energy remain intact in these solvents. The redshifted and broadened absorption spectra in protic solvents likely result from hydrogen-bonding interactions that perturb the donor–acceptor geometry of 4CzIPN, leading to relative ground-state destabilization or excited-state stabilization.

Nanosecond emission dynamics

The prompt and delayed emission of 4CzIPN was characterized using time-correlated single photon counting (TCSPC) measurements. To investigate the role of the H-bonding

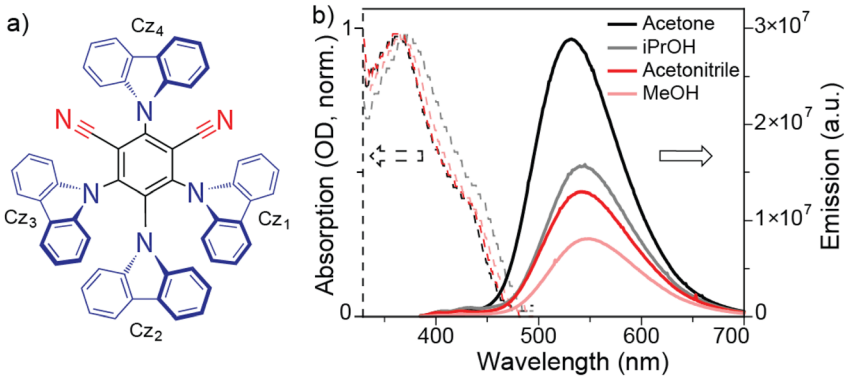

Fig. 2 (a) Chemical structure of 4CzIPN containing four carbazole moieties (Cz_1, Cz_2, Cz_3 and Cz_4). The black and red bonds are in the plane of the paper, whereas the lighter/darker blue bonds indicate the orientation below/above the page. (b) Steady state absorption (dashed line) and emission spectra (solid line) of 4CzIPN in polar aprotic (acetonitrile and acetone) and polar protic solvents (methanol and isopropanol).

environment (protic solvent) in the prompt and delayed components, we recorded TCSPC data (see Fig. 3a) in isopolar aprotic and protic solvents acetonitrile (ACN) and methanol (MeOH) respectively. Fitting the kinetics using the bi-exponential function provides a nanosecond and a microsecond lifetime component which are characteristic of prompt and delayed emission respectively (see Table 2).[22] 4CzIPN in ACN and MeOH shows a prompt lifetime of 18 ns and 10.5 ns respectively while their respective delayed lifetimes are 1.4 μs and 1.3 μs. Therefore the prompt lifetime in protic solvent is significantly quenched (by *ca.* 40%) while the delayed lifetime is nearly unaffected. Such quenching in prompt lifetime resembling the quenching in the overall emission quantum yield supports that the quenching is happening in the excited state. Prompt (Φ_p) and delayed (Φ_d) emission yields were obtained by integrating the respective regions of the time-resolved photoluminescence decay curves and normalizing to the measured total quantum yield (Φ_{total}). This kinetic-area approach, commonly used to deconvolute TADF emission components,[14] allows quantitative estimation of Φ_p and Φ_d. The Φ_p/Φ_d ratios summarized in Table 2 represent the relative contributions of prompt and delayed emission to Φ_{total}. Table 2 shows that the prompt and delayed emission quantum yield values in ACN are 0.15 and 0.05 respectively both of which are quenched to 0.1 and 0.02 respectively in protic MeOH.

To reaffirm the role of the H-bonding environment, we recorded the emission dynamics in isopolar aprotic acetone (ACE) and protic isopropanol (iPrOH) (see SI Fig. S4a) using TCSPC. Fitting the kinetics shows that a prompt lifetime of 24.5 ns in ACE decreases to 15 ns in iPrOH whereas the delayed lifetime values are nearly unchanged (*ca.* 1.58 μs) as shown in Table 2. Therefore H-bonding solvent quenches the prompt lifetime significantly. In addition, the prompt and delayed emission quantum yield values of 0.25 and 0.15 respectively in ACE decrease to 0.19 and 0.05 respectively in iPrOH (see Table 2). Thus both the prompt and delayed emission yield decreases in protic solvent where the effect is more prominent for the latter. To investigate whether there is any contribution of solvent viscosity and polarity in such quenching behaviour, we performed additional TCSPC measurements in methyl acetate (MeOAc), *N*,*N* dimethyl formamide (DMF), and dimethyl acetamide (DMA) (see SI Fig. S4b). Comparing the prompt lifetime values of isoviscous solvents (with increasing solvent polarity) MeOAc, ACE, and ACN, we observe that the prompt lifetimes are 26, 24.5 and 18 ns respectively (see Fig. 3b) while their respective delayed lifetimes are 2, 1.5 and 1.4 μs. Therefore both the prompt and delayed lifetime decreases with an increase in solvent polarity resulting in reduced QY. A gradual decrease in both prompt lifetime and quantum yield by the same factor with increasing solvent polarity in aprotic media is consistent with dipole–dipole interactions between the solvent and the excited 4CzIPN emitter. On the other hand, comparing prompt lifetime values of isopolar solvents (with increasing viscosity) ACN, DMF and DMA, we observe that prompt lifetime values are 18, 23.7 and 28 ns respectively (see Fig. 3b) while the delayed lifetimes remain nearly unchanged (*ca.* 1.5 μs). Therefore the prompt lifetime increases with an increase in solvent viscosity resulting in enhanced overall QY. However the H-bonding solvent shows the opposite trend where protic solvent quenches both the prompt lifetime and overall QY. Therefore protic solvent is playing a crucial role in the quenching of TADF emission.

Table 1 Viscosity, dielectric constant values and protic nature of a range of solvents at 298 K

Properties	ACN	MeOH	Acetone	iPrOH	MeOAc	DMF	DMA
Viscosity (cP)	0.37	0.55	0.32	2	0.38	0.92	1.96
Dielectric constant	37.5	32.6	20.7	18.3	6.6	36.7	37
Protic	No	Yes	No	Yes	No	No	No

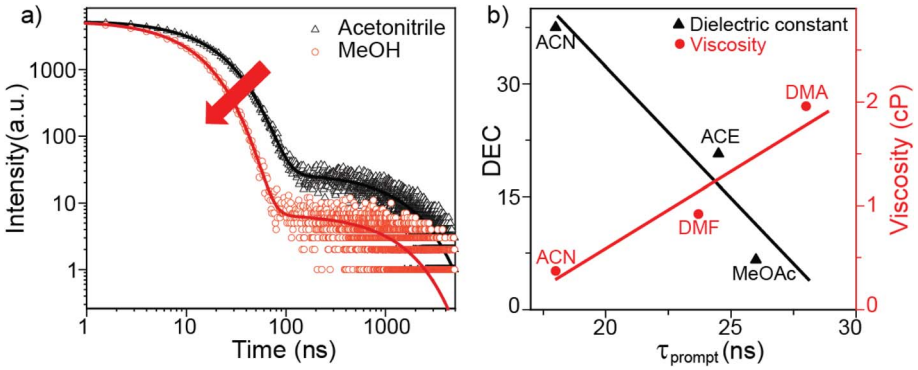

Fig. 3 (a) Nanosecond time-resolved emission decay of 4CzIPN in ACN (black triangles) and MeOH (red circles) obtained using TCSPC. The data were fitted using the biexponential function. (b) The prompt lifetime values have been plotted as a function of the solvent dielectric constant (DEC, black triangles) and viscosity (red circles). The corresponding fittings are shown by solid lines.

Table 2 Prompt (τ_p) and delayed (τ_d) time constant values as obtained from TCSPC measurements are shown. The prompt (Φ_p) and delayed (Φ_d) quantum yield values are determined by fitting the area under the TCSPC kinetic curve

Solvent	QY	τ_p (ns)	τ_d (ns)	φ_p	φ_d	$\varphi_p : \varphi_d$
Acetonitrile	0.2	18	1438.2	0.15	0.05	1 : 0.33
MeOH	0.12	10.5	1384.2	0.10	0.02	1 : 0.16
Acetone	0.4	24.5	1571	0.25	0.15	1 : 0.63
iPrOH	0.24	15	1588	0.19	0.05	1 : 0.24

Femtosecond emission dynamics

In order to investigate the effect of protic solvent in ultrafast emission dynamics of 4CzIPN, we performed femtosecond fluorescence upconversion measurements in isopolar acetonitrile and methanol (see Fig. 4a). Fitting the emission dynamics using the biexponential function provides a nanosecond (instrument limited) and a picosecond component. The long-lived nanosecond component can be assigned to the prompt lifetime as is obtained with the TCSPC data. On the other hand, the ultrafast emission decays at the emission maxima, often manifesting as spectral shifts, are primarily attributed to non-radiative relaxation processes.[36,37] Thus the ultrafast picosecond decay component of 3.15 ps in ACN can be assigned to the nonradiative relaxation timescale as has been reported earlier.[10,22,23,38] Hosokai *et al.* performed transient absorption studies in 4CzIPN to corroborate this timescale to the intramolecular charge transfer.[22] However in protic MeOH, this ultrafast component becomes slower (7.7 ps). A similar behaviour is also observed when we compare the upconversion data in the isopolar solvents, aprotic ACE and protic iPrOH (see SI Fig. S5a). The nonradiative decay time is 3 ps in ACE while it becomes slower (22 ps) in iPrOH. Therefore the nonradiative relaxation time is dependent on the protic environment. To the best of our knowledge, this is the first detailed report of the role of the H-bonding environment in TADF emission.

To investigate the role of solvent polarity and viscosity in the relaxation timescale, we performed additional upconversion measurements in MeOAc, DMF and DMA (see SI Fig. S5b). Fitting emission dynamics in these solvents provide the non-radiative decay time constants of 3.8, 6.3 and 11.8 ps respectively. Comparing the ps-component in isoviscous solvents MeOAc, ACE and ACN suggests that the nonradiative decay timescale is nearly unchanged (*ca.* 3–4 ps) with an increase in solvent polarity (see black triangles in Fig. 4b). On the other hand, on comparing the ps-components in isopolar solvents ACN, DMF and DMA solvents, it is clear that the relaxation timescale increases (from 3.15 to 11.8 ps) with an increase in solvent viscosity (see red circles in Fig. 4b). Therefore the picosecond relaxation timescale is dependent on solvent viscosity, but independent of solvent polarity. Thus the relaxation coordinate associated with FC state decay to form the intramolecular charge transfer state in the ps timescale probably displaces a large volume of solvent. When compared with the nonradiative lifetimes in protic solvents MeOH and iPrOH (red circles in Fig. 4b), we observe that the relaxation process further slows down as indicated by the slope of the fitted line (red dashed line in Fig. 4b) as compared to that in aprotic viscous (red solid line) and polar solvents (black solid line). Therefore a special interaction between protic solvent and 4CzIPN must be contributing to such a decay pathway in protic solvents for slowing down the nonradiative reorganization timescale.

To understand the nature of such ultrafast nonradiative decay, we performed DFT and TDDFT calculations on 4CzIPN which provide the optimized structures in the electronic ground state and excited state, respectively (see Fig. 4c). The molecule contains four carbazole moieties which are on a nearly perpendicular plane with respect to the central aromatic ring. The calculated dihedral angles of all the Cz units in ground and excited state optimized structures are shown in SI Table S4. We observe nearly 10° change in the dihedral angle from the optimized ground state to the optimized excited state geometry which can be assigned to the carbazole torsional relaxation. Such a torsional relaxation in the excited state is supported by the viscosity dependency of time-resolved upconversion measurement (Fig. 4b) where viscous solvent slows down the nonradiative relaxation timescale. Previous reports also highlighted the crucial role of torsional vibrations in mediating the

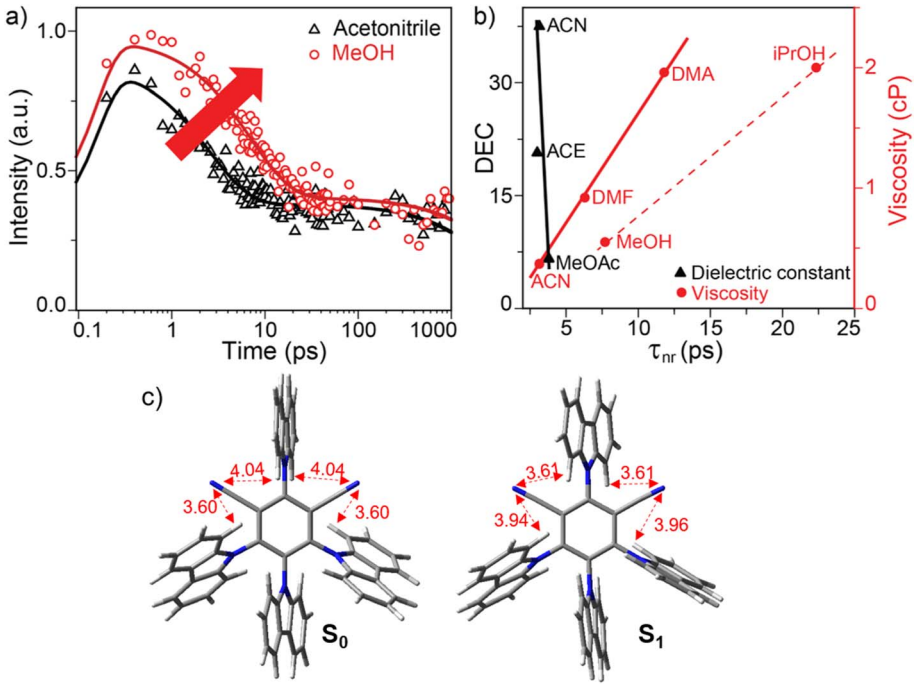

Fig. 4 (a) Femtosecond fluorescence upconversion dynamics of 4CzIPN in ACN (black triangles) and MeOH (red circles). The data were fitted using the biexponential function. (b) The nonradiative decay time constants have been plotted as a function of solvent dielectric constant (DEC, black triangles) and viscosity (red circles). The corresponding fittings are shown by solid lines. (c) DFT and TDDFT calculations on a 4CzIPN molecule provide the ground state (S_0) and excited state (S_1) optimized structures.

spin orbit coupling and spin interconversion.[19,39,40] The calculated nonresonant Raman spectra of the excited state of 4CzIPN shows intense low-frequency vibrational modes at 186, 400, 732 and 780 cm^{-1} (see SI Fig. S6a) which nearly matches with the reported impulsive Raman spectra of the molecule.[10] These modes are mainly coupled ring torsional motions and pyramidal modes of carbazole moieties (as shown in SI Fig. S6b), plausibly driving the formation of charge transfer states.

In protic solvents, further delay in the torsional relaxation timescale suggests a special interaction between the protic solvent and the 4CzIPN molecule. A key question arises: how does a protic solvent slow down the torsional reorganization timescale? One possible explanation is that hydrogen bonding interaction between the protic solvent and 4CzIPN hinders the torsional relaxation of the carbazole (Cz) moieties. Specifically, the interaction likely occurs between the hydroxyl group of the solvent with the C–H hydrogen of the Cz units and the cyano nitrogen in the excited 4CzIPN molecule. This interaction can restrict the rotational freedom of the Cz groups, preventing the molecule from adopting the optimal donor–acceptor (D–A) torsion angle. Consequently, the Franck Condon singlet excited state (S_1^{FC}) undergoes slow relaxation, stabilizing a conformation that exhibits a higher ISC rate and shortened prompt fluorescence lifetime, ultimately suppressing the TADF emission. This is supported by previous work on polar solvation mediated relaxation to a nonemissive state in a different TADF molecule.[19,38] However, the nature of such an H-bonding interaction in 4CzIPN cannot be fully resolved using time-resolved electronic spectroscopic techniques. High-end time-resolved vibrational spectroscopic tools, such as femtosecond IR or Raman spectroscopy, could be employed in future studies to probe these excited state interactions and to capture the detailed structural evolution of the emissive singlets.

To investigate the ground state conformation of 4CzIPN, we recorded single crystal X-ray diffraction (XRD) data as shown in SI Fig. S7. Here all four carbazole (Cz) moieties are nearly at a perpendicular dihedral angle with respect to the central benzene ring. The shortest N···H distance of 0.32 nm is observed between nitrogen of the cyano group and the nearest hydrogen of the Cz-1 unit. This indicates very weak intramolecular H-bonding interaction present in the ground state of 4CzIPN. Such weak intramolecular H-bonding was also observed in other TADF molecules utilizing single crystal XRD.[28,29,41] The distance between N of the cyano group and the nearest H of the Cz-4 unit in 4CzIPN is 0.4 nm. This observation is also supported by DFT calculation where we observed the shortest N···H distance of 0.36 nm between the CN and Cz-1 unit (see Fig. 4c) whereas the N···H distance between CN and the Cz-4 unit is 0.4 nm. However in the excited state optimized structure (as obtained from TDDFT calculation), the N···H distance between CN and Cz-1 groups is 0.39 nm while the shortest N···H distance of 0.36 nm is observed between nitrogen of the CN group and the nearest hydrogen of the Cz-4 moiety. This clearly suggests that the nature of the intramolecular interaction changes from the ground state to the excited state driven by the large dipole moment of the excited state.

In the presence of a protic solvent, such intramolecular H-bonding will be affected as the solvent hydroxyl groups could interact with both the cyano nitrogen and carbazole hydrogens in the electronic ground and excited state of 4CzIPN. To investigate the solvent interaction in the ground state, NMR data of 4CzIPN were recorded in ACN with different percentages of isopolar MeOH (see SI Fig. S8). The peak at 112.2 ppm corresponds to cyano carbon which is upfield shifted with the addition of methanol. The peaks at 110.64 and 110.55 correspond to the nearest carbons of the carbazole-1 and 4 respectively which also get upfield shifted with the addition of methanol. A similar behaviour of NMR peakshift was also observed when isopropanol was added in the acetone solution of 4CzIPN (see SI Fig. S9). Such solvent-dependent NMR peak shifts indicate structural perturbation of the ground-state 4CzIPN in methanol, despite its polarity being comparable to that of acetonitrile. Since aprotic acetonitrile is very unlikely to form any hydrogen-bonding interaction[42] with 4CzIPN, the observed changes can be attributed to weak hydrogen-bonding interactions between protic methanol and 4CzIPN. Explicit solvation-model DFT calculations further support this, revealing potential hydrogen-bonding interaction sites in the ground state. In these calculations, a methanol molecule was placed at different plausible interaction sites of 4CzIPN (Models 1–3, see SI Fig. S10–S12), and first optimized in the ground state using DFT. The optimized geometries show the N···H hydrogen-bond distances of 2.11 Å between the methanol hydroxyl hydrogen and the cyano nitrogen of 4CzIPN. Moreover O···H distances of ∼2.4 Å between methanol oxygen and carbazole hydrogens suggest additional interactions at these sites. Notably, these interactions also induce measurable variations in the carbazole dihedral angles (SI Model 1–3 in Fig. S10–S12) relative to the gas-phase optimized DFT structures (SI Table S4). Collectively, these results confirm that both N···H and O···H interactions are operative in the ground state. Such an interaction is modulating the ground state structure and ring electronics and hence possibly contributing towards the redshifted absorption in protic solvent (as discussed in Fig. 2b).

Role of deuterated solvent

To substantiate the involvement of hydrogen-bonding interactions between methanol and 4CzIPN in the excited state, steady-state and time-resolved photoluminescence measurements were carried out in deuterated methanol (MeOD). In MeOD, the emission quantum yield and prompt lifetime of 4CzIPN were found to be 0.19 and 13.6 ns, respectively—showing ∼1.3 fold enhancement relative to normal methanol (MeOH), while the delayed lifetime remained nearly unchanged (see Fig. 5). This kinetic isotope effect unequivocally supports the involvement of solvent protons in hydrogen-bonding interactions with photo-excited 4CzIPN, influencing its excited-state energetics and dynamics. Such interactions with protic solvents likely promote enhanced intersystem crossing (ISC) and reduced reverse ISC (rISC) by modulating the donor–acceptor dihedral angle. To elucidate the potential hydrogen-bonding interaction sites in the excited states, explicit solvation-model TDDFT calculations

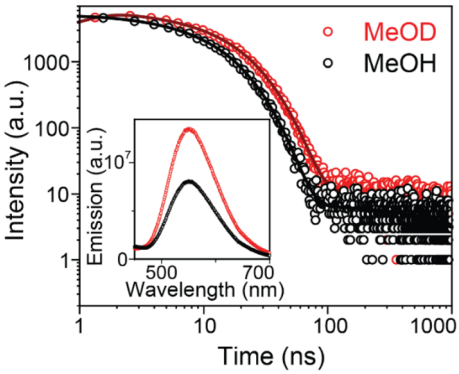

Fig. 5 Nanosecond emission dynamics of 4CzIPN (circles) and corresponding fits (solid lines) in normal methanol (black) and deuterated methanol (red) are shown. The inset shows TADF emission spectra in deuterated methanol (red) relative to normal methanol (black).

were performed on the ground state optimized geometries. Upon excited state optimization (see SI Fig. S10–S12), the hydrogen-bond distance between the methanol O–H hydrogen and the cyano nitrogen of 4CzIPN decreases relative to the ground-state (DFT) geometry, indicating a stronger hydrogen-bonding interaction in the excited state. In contrast, the O···H distances between the methanol oxygen and carbazole hydrogens exhibit minor variations, suggesting additional but weaker stabilization at these sites. These interactions also induce noticeable changes in the carbazole dihedral angles of the TDDFT-optimized structures (SI Model 1–3, Fig. S10–S12) compared to the gas-phase excited-state geometry (SI Table S4). Collectively, these results indicate that both N···H and O···H interactions become more favorable in the excited state, providing theoretical support for our experimental observation of pronounced solvent-dependent behavior in protic environments.

Discussion

The combined results of all the time-resolved studies provide a comprehensive answer to the question of why does emission and lifetime quenching occur in protic solvents. The timescale and quantum yield of prompt emission depends upon the rate constants of ISC (k_{isc}), and radiative (k_r) and nonradiative (k_{nr}) decays of the singlet.[43] The k_r of 4CzIPN in aprotic ACN and protic MeOH is 8.3×10^6 s^{-1} and 9.5×10^6 s^{-1} respectively as determined from the ratio of prompt quantum yield and prompt lifetime values in these solvents. Therefore, the radiative rate constant remains nearly unaffected, suggesting that the intrinsic nature of the emissive state is preserved across these solvents. Ishimatsu *et al.* reported that the k_{nr} varies negligibly between isopolar protic and aprotic solvents.[14] Using these parameters, k_{ISC} and k_{rISC} were estimated (summarized in SI Table S1) following established methods.[2,14] We observed nearly a ∼38-fold increase in k_{ISC} and a ∼11-fold decrease in k_{rISC} in methanol relative to acetonitrile. The enhanced k_{ISC} likely originates from hydrogen-bonding–induced modulation of the donor–acceptor dihedral angle, which facilitates faster singlet-

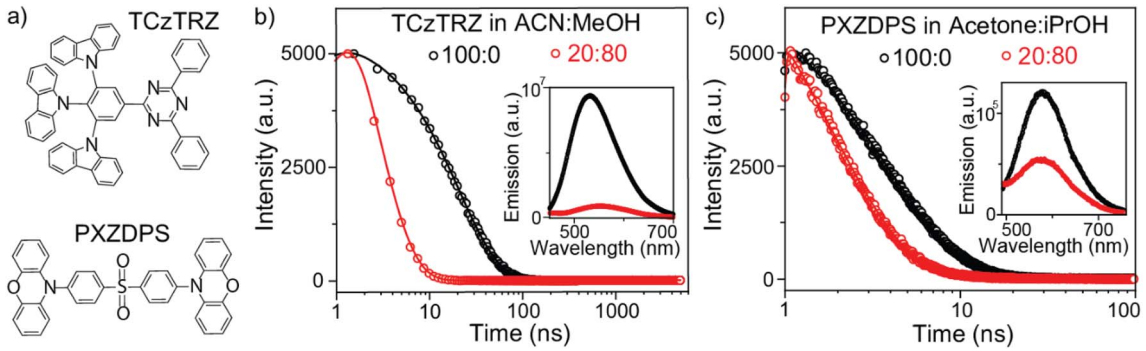

Fig. 6 (a) Chemical structures of TCzTRZ and PXZDPS. The nanosecond emission dynamics of (b) TCzTRZ in pure acetonitrile (black) and a 20 : 80 (v/v) acetonitrile/methanol mixture (red) and (c) PXZDPS in pure acetone (black) and a 20 : 80 (v/v) acetone/isopropanol mixture (red). Insets show the corresponding steady-state emission spectra in these solvent environments.

to-triplet conversion.[24–26] Conversely, the suppressed k_{rISC} can be attributed to an increased singlet–triplet energy gap (ΔE_{ST}), reported to increase from 98 meV in ACN to 110 meV in ethanol.[14] As a consequence, a larger fraction of excitons becomes trapped in the triplet manifold where they undergo nonradiative decay instead of being converted back into emissive singlets. This altered balance between forward and reverse intersystem crossing simultaneously suppresses both Φ_p and Φ_d, shortens the prompt lifetime, and leaves the delayed lifetime almost unchanged—providing a comprehensive mechanistic rationale for the substantial quenching of TADF emission in protic environments. Therefore, H-bonding interactions with protic solvents lead to an excited electronic state with an increased ISC and a reduced rISC rate constant possibly by modulating the D–A dihedral angle.

To further validate the generality of the observed solvent-dependent behavior, we extended our investigation to two additional TADF emitters—9,9′,9″-(5-(4,6-diphenyl-1,3,5-triazin-2-yl)benzene-1,2,3-triyl)tris(9*H*-carbazole) (TCzTRZ) and 10,10′-(sulfonylbis(4,1-phenylene))bis(10*H*-phenoxazine) (PXZDPS)—featuring distinct donor–acceptor frameworks and electronic structures (see Fig. 6a).[44,45] Steady-state and time-resolved emission measurements were performed for these molecules in isopolar protic and aprotic solvent pairs (ACN-MeOH; acetone-iPrOH). Remarkably, both emitters exhibit a pronounced reduction in emission intensity and lifetime when transferred from aprotic to protic environments, mirroring the trend observed for 4CzIPN. For TCzTRZ, the photoluminescence quantum yield decreases by 87% in methanol (Fig. 6b inset), accompanied by a drop in prompt lifetime from 20.7 ns to 2.4 ns (Fig. 6b). Likewise, PXZDPS shows a 49% reduction in quantum yield (Fig. 6c inset) along with a decrease in lifetime from 3.8 ns to 1.8 ns (Fig. 6c) when acetone is replaced with iPrOH. This consistent quenching across chemically diverse TADF emitters highlights the dominant role of hydrogen-bonding interactions in facilitating nonradiative decay processes in protic solvents. Such interactions likely perturb the donor–acceptor geometry and modulate the excited state electronic structure, leading to enhanced intersystem crossing and reduced reverse intersystem crossing rates. Collectively, these results establish that hydrogen-bonding-induced excited-state quenching is a general and intrinsic phenomenon among multidonor–acceptor TADF systems rather than a molecule-specific effect.

Conclusion

In summary, we demonstrate that hydrogen-bonding interactions with the surrounding medium act as a universal quencher of TADF emission. A clear kinetic isotope effect confirms that solvent protons directly participate in these excited state interactions, selectively suppressing the prompt fluorescence channel while leaving delayed lifetimes largely unaffected. Here

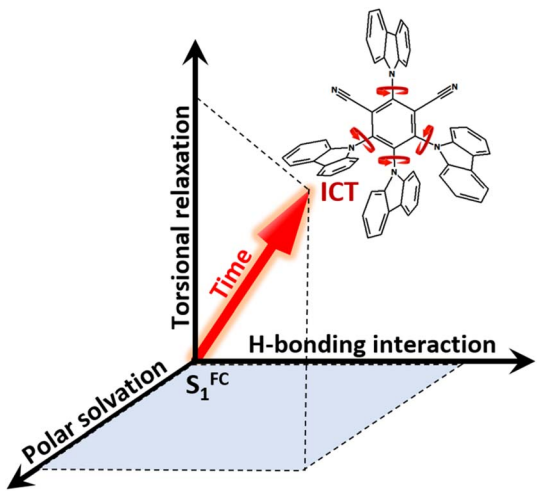

Fig. 7 Excited state evolution of 4CzIPN. Upon photoexcitation, 4CzIPN populates the Franck–Condon singlet excited state (S_1^{FC}), which subsequently relaxes along multiple coordinates, including polar solvation, torsional relaxation, and hydrogen-bonding interactions, depending on the surrounding solvent environment. This results in an intramolecular charge transfer state (ICT) where the molecular conformation plays a crucial role in dictating the rate and efficiency of subsequent processes such as intersystem crossing (ISC), reverse intersystem crossing (rISC), and radiative decay. In H-bonding solvent, the S_1^{FC} state undergoes slow relaxation, stabilizing a conformation that exhibits shorter-lived excited states, ultimately suppressing the TADF emission.

we resolve the complex dependency of the solvent environment on the excited state dynamics of the TADF molecule. Photoexcitation of 4CzIPN leads to the Franck Condon excited singlet state (S_1^{FC}) which undergoes picosecond relaxation along multiple coordinates, including polar solvation, torsional relaxation, and hydrogen-bonding interactions depending on the nature of the surrounding medium (see Fig. 7). This leads to an intramolecular charge transfer (ICT) state where the conformation of donor–acceptor units plays a pivotal role in dictating the rate and efficiency of subsequent processes such as intersystem crossing (ISC), reverse intersystem crossing (rISC), and radiative decay. Viscosity dependency on the ps emission decay along with excited state calculation suggest the critical role of carbazole ring torsion in driving relaxation of the S_1^{FC} state in this timescale. In viscous solvent, the torsional relaxation is hindered leading to an emissive singlet state with longer prompt lifetime. In protic solvent, this relaxation time further slows down leading to a relaxed ICT state that has been characterized with shorter prompt lifetime and significantly reduced emission quantum yield. Complementary explicit-solvation model calculations further reveal the key interaction sites on the photoexcited emitter and provide a mechanistic basis for the observed photophysical changes. In the future, advanced time-resolved vibrational spectroscopic techniques, combined with quantum mechanical calculations, could provide detailed insights into the excited state structural evolution. Our results pave the way for tuning the microenvironment that complements TADF emission through tailored additives, with direct implications for next-generation display technologies and photocatalysis.

Methods

(i) Spectroscopy: the time-resolved methods used here for TCSPC[46,47] and fluorescence up-conversion,[48] have all been described elsewhere and are further detailed in the SI. The steady-state spectroscopic measurements are also detailed in the SI.

(ii) Computational details: all DFT and TDDFT calculations of 4CzIPN were carried out using Gaussian16.[49] The ground state geometry optimization and the non-resonant Raman spectral calculations were performed using the DFT method at the RB3LYP/TZVP level. The excited state geometry and Raman frequency were optimized using the TDDFT method with the cam-B3LYP functional, 6-31G(d,p) basis set. All frequencies have been scaled to account for a systematic error in the DFT predictions. The methodology for explicit solvation model DFT/TDDFT calculations are provided in the SI.

Author contributions

PR conceived the project and wrote the draft. SSP and LD collected steady-state and time-resolved data. SSP analysed the data in discussion with PR. PR and LD performed DFT/TDDFT calculations. All authors have given approval to the final version of the manuscript.

Conflicts of interest

The authors declare no conflict of interest.

Data availability

The data that support the findings of this study are available in the paper and supplementary information (SI). Supplementary Information: details of the experimental methods, additional figures and tables. See DOI: https://doi.org/10.1039/d5sc05548b.

Acknowledgements

We acknowledge the IIT Bhubaneswar seed grant and Anusandhan National Research Foundation (ANRF) grant (ANRF/ECRG/2024/000854/CS) for generous financial support. PR is grateful to Prof. Himansu Biswal, Dr Subhadip Ghosh and NISER Bhubaneswar for support in performing the time-resolved emission measurements. SSP thanks Mr Chandan Kumar, Mr Shubhendu Patra and Ms. Subhashree Kar for help in the steady-state experiments.

References

1 H. Nakanotani, Y. Tsuchiya and C. Adachi, *Chem. Lett.*, 2021, **50**, 938–948.
2 H. Uoyama, K. Goushi, K. Shizu, H. Nomura and C. Adachi, *Nature*, 2012, **492**, 234–238.
3 Y. Sun, N. C. Giebink, H. Kanno, B. Ma, M. E. Thompson and S. R. Forrest, *Nature*, 2006, **440**, 908–912.
4 P. K. Samanta, D. Kim, V. Coropceanu and J.-L. Brédas, *J. Am. Chem. Soc.*, 2017, **139**, 4042–4051.
5 Z. Zhao, S. Yan and Z. Ren, *Acc. Chem. Res.*, 2023, **56**, 1942–1952.
6 T. Chatterjee and K. T. Wong, *Adv. Opt. Mater.*, 2019, **7**, 1800565.
7 S. Oner and M. R. Bryce, *Mater. Chem. Front.*, 2023, **7**, 4304–4338.
8 E. Cho, M. Hong, V. Coropceanu and J. L. Brédas, *Adv. Opt. Mater.*, 2021, **9**, 2002135.
9 J.-H. Jou, S. Kumar, A. Agrawal, T.-H. Li and S. Sahoo, *J. Mater. Chem. C*, 2015, **3**, 2974–3002.
10 A. J. Gillett, A. Pershin, R. Pandya, S. Feldmann, A. J. Sneyd, A. M. Alvertis, E. W. Evans, T. H. Thomas, L.-S. Cui and B. H. Drummond, *Nat. Mater.*, 2022, **21**, 1150–1157.
11 Y. Olivier, B. Yurash, L. Muccioli, G. D'Avino, O. Mikhnenko, J.-C. Sancho-Garcia, C. Adachi, T.-Q. Nguyen and D. Beljonne, *Phys. Rev. Mater.*, 2017, **1**, 075602.
12 X. Xiao, Y. Yan, A. A. Sukhanov, S. Doria, A. Iagatti, L. Bussotti, J. Zhao, M. Di Donato and V. K. Voronkova, *J. Phys. Chem. B*, 2023, **127**, 6982–6998.
13 M. Aydemir, G. Haykır, F. Türksoy, S. Gümüş, F. B. Dias and A. P. Monkman, *Phys. Chem. Chem. Phys.*, 2015, **17**, 25572–25582.
14 R. Ishimatsu, S. Matsunami, K. Shizu, C. Adachi, K. Nakano and T. Imato, *J. Phys. Chem. A*, 2013, **117**, 5607–5612.

15 W. Whitaker, I. V. Sazanovich, Y. Kwon, W. Jeon, M. S. Kwon and A. J. Orr-Ewing, *J. Phys. Chem. A*, 2023, **127**, 10775–10788.
16 M. A. Bryden and E. Zysman-Colman, *Chem. Soc. Rev.*, 2021, **50**, 7587–7680.
17 S. Grotjahn and B. König, *Chem. Commun.*, 2024, **60**, 12951–12963.
18 H. Noda, H. Nakanotani and C. Adachi, *Sci. Adv.*, 2018, **4**, eaao6910.
19 I. E. Serdiuk, C. H. Ryoo, K. Kozakiewicz, M. Mońka, B. Liberek and S. Y. Park, *J. Mater. Chem. C*, 2020, **8**, 6052–6062.
20 S. Debnath, P. Ramkissoon, U. Salzner, C. R. Hall, N. A. Panjwani, W. Kim, T. A. Smith and S. Patil, *Nat. Commun.*, 2025, **16**, 2982.
21 I. S. Park, K. Matsuo, N. Aizawa and T. Yasuda, *Adv. Funct. Mater.*, 2018, **28**, 1802031.
22 T. Hosokai, H. Matsuzaki, H. Nakanotani, K. Tokumaru, T. Tsutsui, A. Furube, K. Nasu, H. Nomura, M. Yahiro and C. Adachi, *Sci. Adv.*, 2017, **3**, e1603282.
23 J. Lu, B. Pattengale, Q. Liu, S. Yang, W. Shi, S. Li, J. Huang and J. Zhang, *J. Am. Chem. Soc.*, 2018, **140**, 13719–13725.
24 J. Gibson, A. P. Monkman and T. J. Penfold, *ChemPhysChem*, 2016, **17**, 2956–2961.
25 K. Suzuki and H. Kaji, *J. Am. Chem. Soc.*, 2023, **145**, 16324–16329.
26 F. B. Dias, J. Santos, D. R. Graves, P. Data, R. S. Nobuyasu, M. A. Fox, A. S. Batsanov, T. Palmeira, M. N. Berberan-Santos and M. R. Bryce, *Adv. Sci.*, 2016, **3**, 1600080.
27 J. Pandidurai, J. Jayakumar, N. Senthilkumar and C.-H. Cheng, *J. Mater. Chem. C*, 2019, **7**, 13104–13110.
28 W. Yuan, H. Yang, C. Duan, X. Cao, J. Zhang, H. Xu, N. Sun, Y. Tao and W. Huang, *Chem*, 2020, **6**, 1998–2008.
29 Y. Guo, L. Hua, H. Zhao, Y. Liu, S. Yan and Z. Ren, *J. Phys. Chem. C*, 2024, **128**, 11924–11932.
30 Y. Guo, Y. Gao, J. Zhang, C. Wang, Y. Wang, X. Feng and G. Zhao, *J. Phys. Chem. C*, 2023, **127**, 4784–4791.
31 M. Hempe, N. A. Kukhta, A. Danos, A. S. Batsanov, A. P. Monkman and M. R. Bryce, *J. Phys. Chem. Lett.*, 2022, **13**, 8221–8227.
32 H. Yang, Q. Liang, C. Han, J. Zhang and H. Xu, *Adv. Mater.*, 2017, **29**, 1700553.
33 F. Gao, R. Du, F. Jiao, G. Lu, J. Zhang, C. Han and H. Xu, *Adv. Opt. Mater.*, 2020, **8**, 2000052.
34 Y. Tian, H. Wang, Y. Man, N. Zhang, J. Zhang, Y. Li, C. Han and H. Xu, *Chem. Sci.*, 2021, **12**, 14519–14530.
35 A. C. Brannan, E. F. P. Beaumont, N. L. Phuoc, G. F. S. Whitehead, M. Linnolahti and A. S. Romanov, *Beilstein J. Org. Chem.*, 2023, **19**, 1289–1298.
36 M. Glasbeek and H. Zhang, *Chem. Rev.*, 2004, **104**, 1929–1954.
37 P. Abbyad, W. Childs, X. Shi and S. G. Boxer, *Proc. Natl. Acad. Sci. U. S. A.*, 2007, **104**, 20189–20194.
38 Z. Kuang, G. He, H. Song, X. Wang, Z. Hu, H. Sun, Y. Wan, Q. Guo and A. Xia, *J. Phys. Chem. C*, 2018, **122**, 3727–3737.
39 E. W. Evans, Y. Olivier, Y. Puttisong, W. K. Myers, T. J. Hele, S. M. Menke, T. H. Thomas, D. Credgington, D. Beljonne and R. H. Friend, *J. Phys. Chem. Lett.*, 2018, **9**, 4053–4058.
40 M. K. Etherington, J. Gibson, H. F. Higginbotham, T. J. Penfold and A. P. Monkman, *Nat. Commun.*, 2016, **7**, 13680.
41 Y. Z. Shi, K. Wang, X. C. Fan, J. X. Chen, X. M. Ou, J. Yu, J. S. Jie, C. S. Lee and X. H. Zhang, *Adv. Opt. Mater.*, 2021, **9**, 2100461.
42 M. I. Sancho, M. C. Almandoz, S. E. Blanco and E. A. Castro, *Int. J. Mol. Sci.*, 2011, **12**, 8895–8912.
43 K. Goushi, K. Yoshida, K. Sato and C. Adachi, *Nat. Photonics*, 2012, **6**, 253–258.
44 Q. Zhang, B. Li, S. Huang, H. Nomura, H. Tanaka and C. Adachi, *Nat. Photonics*, 2014, **8**, 326–332.
45 S. Y. Byeon, J. Kim, D. R. Lee, S. H. Han, S. R. Forrest and J. Y. Lee, *Adv. Opt. Mater.*, 2018, **6**, 1701340.
46 D. Acharjee, A. B. Mahato, A. Das and S. Ghosh, *J. Phys. Chem. C*, 2023, **127**, 19643–19650.
47 N. Preeyanka, T. Goswami, R. Saha, A. Akhuli, A. K. Dehury and M. Sarkar, *J. Phys. Chem. C*, 2022, **126**, 15838–15848.
48 K. Mishra, D. Acharjee, A. Das and S. Ghosh, *J. Phys. Chem. B*, 2021, **125**, 11017–11025.
49 M. J. Frisch, G. W. Trucks, H. B. Schlegel, G. E. Scuseria, M. A. Robb, J. R. Cheeseman, G. Scalmani, V. Barone, G. A. Petersson, H. Nakatsuji, X. Li, M. Caricato, A. V. Marenich, J. Bloino, B. G. Janesko, R. Gomperts, B. Mennucci, H. P. Hratchian, J. V. Ortiz, A. F. Izmaylov, J. L. Sonnenberg, D. Williams-Young, F. Ding, F. Lipparini, F. Egidi, J. Goings, B. Peng, A. Petrone, T. Henderson, D. Ranasinghe, V. G. Zakrzewski, J. Gao, N. Rega, G. Zheng, W. Liang, M. Hada, M. Ehara, K. Toyota, R. Fukuda, J. Hasegawa, M. Ishida, T. Nakajima, Y. Honda, O. Kitao, H. Nakai, T. Vreven, K. Throssell, J. A. Montgomery Jr, J. E. Peralta, F. Ogliaro, M. J. Bearpark, J. J. Heyd, E. N. Brothers, K. N. Kudin, V. N. Staroverov, T. A. Keith, R. Kobayashi, J. Normand, K. Raghavachari, A. P. Rendell, J. C. Burant, S. S. Iyengar, J. Tomasi, M. Cossi, J. M. Millam, M. Klene, C. Adamo, R. Cammi, J. W. Ochterski, R. L. Martin, K. Morokuma, O. Farkas, J. B. Foresman and D. J. Fox, *Gaussian 16, Revision A.03*, Gaussian, Inc., Wallingford CT, 2016.